Tuning of ferrimagnetism and perpendicular magnetic anisotropy in $NiCo_2O_4$ epitaxial films by the cation distribution

Yufan Shen,[1] Daisuke Kan,[1,*] Zhenhong Tan,[1] Yusuke Wakabayashi,[2] and Yuichi Shimakawa[1,3]

[1]*Institute for Chemical Research, Kyoto University, Uji, Kyoto 611-0011, Japan*

[2]*Department of Physics, Graduate School of Science, Tohoku University, Sendai 980–8578, Japan*

[3]*Integrated Research Consortium on Chemical Sciences, Uji, Kyoto 611-0011, Japan*

(Received 9 October 2019; revised manuscript received 5 February 2020; accepted 27 February 2020; published 11 March 2020)

Cation distribution in transition-metal oxides is closely tied to their physical properties. Here we employed resonant x-ray-diffraction technique and quantitatively evaluated the cation distribution in inverse spinel $NiCo_2O_4$ films that were epitaxially grown by pulsed laser deposition. Our results reveal that oxygen partial pressure during growth P_{O2} is a key parameter determining cation distribution in the films, with a larger P_{O2} leading to an increase in the Ni concentration occupying the octahedral (O_h) sites. We further show that the P_{O2}-dependent O_h-site Ni concentration impacts the magnetic properties of the films: Films having the cation distribution close to the stoichiometric exhibit ferrimagnetism with a transition temperature higher than 400 K and enhanced perpendicular magnetic anisotropy. On the other hand, the reductions in the O_h-site Ni concentration leads to the deterioration of the ferrimagnetic properties such as magnetization, transition temperature, and anisotropy energy. Our study demonstrates that the ferrimagnetic properties and the anisotropy can be tuned through the cation distribution, which would provide an additional degree of freedom in designing spintronic devices based on spinel oxides including $NiCo_2O_4$.

DOI: 10.1103/PhysRevB.101.094412

I. INTRODUCTION

Transition-metal oxides can accommodate various types of cation arrangements, such as (dis-)orderings and distributions, leading to richness in functional properties. For ternary spinel oxides AB_2O_4, cation distributions over two crystallographically distinct sites, at which cations are tetrahedrally and octahedrally coordinated by the oxygen, have been shown to significantly influence physical properties such as electrical conductivity, magnetism, and thermoelectric properties [1–9]. It is therefore important to delineate how the cation composition and distribution influence properties of spinel oxides and how the distribution can be controlled.

The inverse spinel oxide $NiCo_2O_4$ (NCO) [10–14], whose tetrahedral (T_d) site is occupied by Co and octahedral (O_h) site is equally populated by Ni and Co [Fig. 1(a)], is known to be a ferrimagnet with a transition temperature above 400 K and a saturated magnetization of $1.5 \sim 2\mu_B$ formula unit (f.u.). This oxide has been shown to exhibit a variety of physical properties such as electrochemical activity [15–18], metallic electrical conduction [8,19–21], and perpendicular magnetic anisotropy [22], attracting a great deal of attention. Recent investigations of NCO epitaxial thin films revealed that their magnetic and transport properties strongly depend on growth conditions such as growth temperatures, oxygen partial pressure during film growth, and postannealing [8,10,23–25]. These studies suggest that the cation distribution and composition in NCO films deviates from the ideal one in ways depending on growth conditions. Given possible variations of cation distribution and valence states of Ni and Co in NCO (Supplemental Material, Fig. S1 [26]), such deviations would result in modifications in films' physical properties. However, because the x-ray scattering amplitudes (the Thomson scattering term) of Co and Ni are very similar, conventional x-ray-diffraction techniques are not able to distinguish these cations and quantitatively evaluating cation distribution (the cation compositions in the T_d and O_h sites) in film specimens is still challenging. Moreover, delineating how film-growth conditions influence the cation distribution in NCO films and elucidating how the cation distribution affects films' properties remain elusive.

In this study, we employed resonant x-ray-diffraction technique [8,27–30] and quantitatively evaluated the cation distribution in NCO films grown under various oxygen partial pressures (P_{O2}) by pulsed laser deposition. By tuning the incident x-ray energy to given absorption edges of Co and Ni, anomalous scattering is enhanced and modifies diffraction intensities from the films. Reproducing such intensity modifications under resonant conditions allows us to quantify compositions of elements contributing to observed diffraction intensity, and consequently to determine cation composition and distribution in the films. We found that the cation distribution close to the stoichiometric is seen for the films grown under higher P_{O2}. On the other hand, depositing NCO under lower P_{O2} leads to deviations in the cation distribution: an increase in the Ni concentration in the T_d site and a decrease in the Ni concentration in the O_h site. This indicates that varying

*dkan@scl.kyoto-u.ac.jp

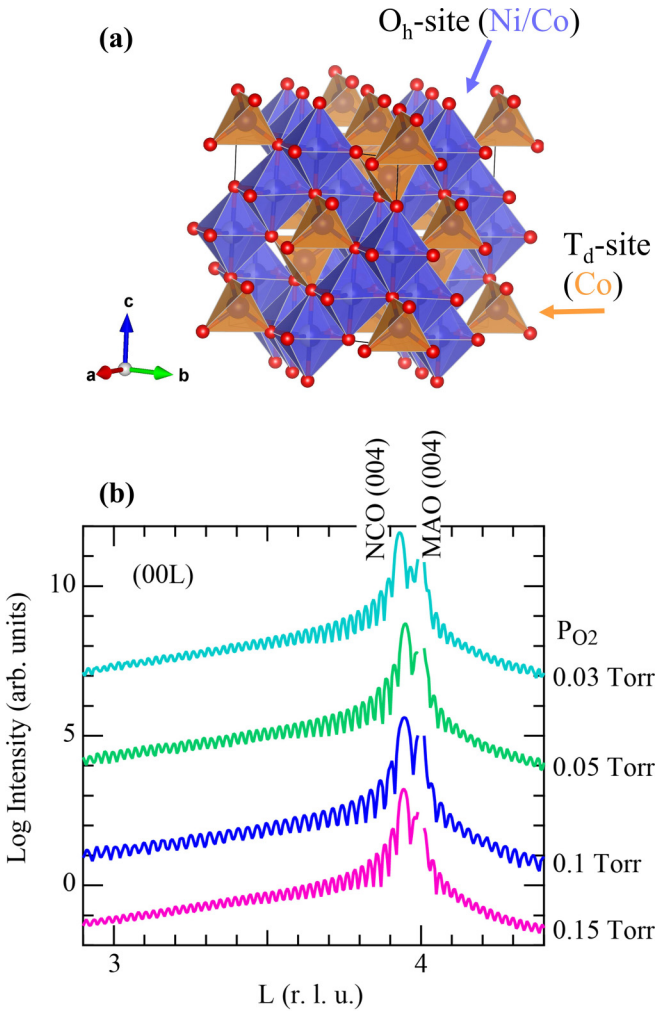

FIG. 1. (a) Crystal structure of the inverse spinel oxide $NiCo_2O_4$. (b)Nonresonant (00L) x-ray-diffraction profiles for NCO films grown under various P_{O2}. The data were obtained with an 8-keV x-ray incident beam. The thicknesses determined for the period of the thickness fringes are 33, 26, 33, and 33 nm for the films grown under $P_{O2} = 0.15, 0.1, 0.05$, and 0.03 Torr, respectively. Note that the substrate peaks are not included in the profiles.

P_{O2} is useful in tuning the cation distribution in NCO. We also show that the cation distributions due to the variations in P_{O2} significantly influence their above-room-temperature ferrimagnetism, including the magnetization, the transition temperature, and the perpendicular magnetic anisotropy. Our observations highlight that tuning the cation distribution in NCO films is a useful way of controlling their ferrimagnetic properties and perpendicular magnetic anisotropy.

II. EXPERIMENTAL DETAILS

Epitaxial thin films of NCO were grown on (001) $MgAl_2O_4$ (MAO) substrates by pulsed laser deposition (PLD). Based on the lattice parameters of NCO ($a_{NCO} = 8.11$ Å) and MAO ($a_{MAO} = 8.08$ Å) in bulk, films experience the compressive strain of ~0.4% due to the lattice mismatch. The films were deposited by ablating a $NiCo_2O_x$ ceramic target at 6 Hz with a KrF excimer laser ($\lambda = 248$ nm) with a laser spot density of 1.2 J/cm^2, at the fixed substrate temperature of 350°C, and under various oxygen partial pressures ($P_{O2} = 0.03, 0.05, 0.1$, and 0.15 Torr). After the film growth, the films were cooled down to room temperature without changing P_{O2}.

Structural properties of the films were characterized by laboratory-source and synchrotron x-ray diffraction. The laboratory-source x-ray $2\theta/\theta$ diffraction measurements and reciprocal space mappings (PANalytical X'Pert MRD) confirmed that regardless of the P_{O2}, the NCO layers were coherently grown on the substrates and the in-plane lattice constants of the NCO layers were identical to those of the substrates. Synchrotron x-ray-diffraction measurements, including those of the incident x-ray energy dependence of the NCO reflection intensities, were carried out at the BL-4C in the Photon Factory.

Magnetization of the films was measured using superconducting quantum interference device magnetometry. The electrical resistivity ρ_{xx} of the films was measured by a van der Pauw method. To measure the transverse (Hall) resistivity ρ_{xy} in a conventional four-terminal configuration, the fabricated films were patterned into 50-μm-wide Hall bars by conventional photolithography and Ar-ion milling. The anomalous Hall resistivity was extracted by antisymmetrizing the measured ρ_{xy} and then subtracting the normal part from the antisymmetrized ρ_{xy}.

III. RESULTS AND DISCUSSION

We grew 26–33-nm-thick NCO films on (001) $MgAl_2O_4$ (MAO) substrates by PLD. Laboratory-source x-ray $2\theta/\theta$ diffraction and reciprocal space mapping measurements (Figure S2 in the Supplemental Material [26]) confirmed that all the films were (001) oriented with the out-of-plane lattice constants slightly longer than the bulk and the in-plane lattice constants of the films were fixed by the substrate's lattice. This indicates that the films were under substrate-induced compressive strain.

We further performed synchrotron x-ray-diffraction characterizations for the NCO films. Measurements were carried out at the BL-4C in the Photon Factory. Figure 1(b) shows (00L) profiles for the film grown under $P_{O2} = 0.03, 0.05, 0.1$, and 0.15 Torr. The profiles were obtained with the 8-keV incident x-ray beam. Regardless of the P_{O2}, all NCO films exhibit (00L) Bragg reflections together with the clear thickness fringes, which ensures highly uniform and sharp interfaces of the grown films. We also note that no reflections originating from (111)-oriented NCO layers or secondary phases are seen.

To quantitatively evaluate the cation distribution of Co ($Z = 27$) and Ni ($Z = 28$) in the films, we carried out resonant x-ray-diffraction measurements. It should also be pointed out that for the (inverse) spinel structure, cations occupying in the T_d and O_h sites have distinct contributions on certain Bragg reflections (for details, please see Table 1S in the Supplemental Material [26]). For example, the (022) reflection intensity originates only from scatterings by the T_d cations, whereas the (222) reflection intensity originates only from scattering by O_h cations. It should be noted that this site dependence of the cation contribution to the diffraction intensities holds even when the unit cell is deformed, as in the case for

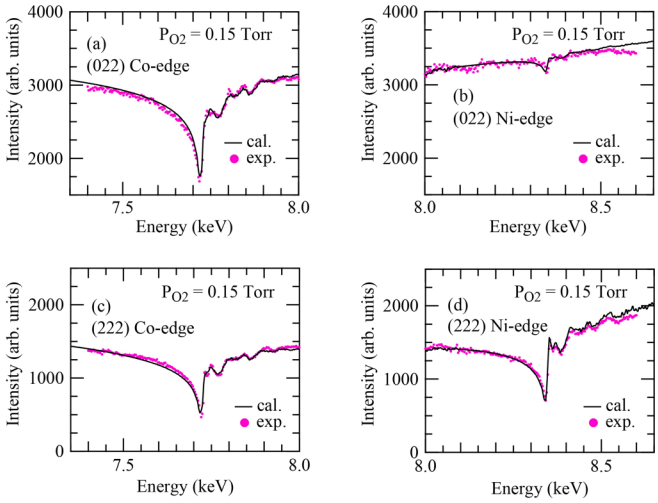

FIG. 2. (a), (b) Measured and calculated energy dependence of the (022) NCO reflection intensities around (a) Co-K and (b) Ni-K absorption edges for the $P_{O2} = 0.15$ Torr film. (c), (d) Measured and calculated energy dependence of the (222) NCO reflection intensities around (c) Co-K and (d) Ni-K absorption edges for the $P_{O2} = 0.15$ Torr film.

the compressively strained $NiCo_2O_4$ films (no changes in cations' internal coordination in the unit cell are assumed). Although oxygens have finite but small contributions to these reflections, interferences between scatterings from cations and oxygens are weak. Therefore, tracking how these reflection intensities vary under resonance conditions for Co and Ni and reproducing the experimentally observed reflection intensities by structural model calculations allow one to quantify the site distributions of the cations in the NCO films. Figures 2(a)–2(d) summarize the incident x-ray energy dependence of the (022) and (222) NCO reflections for the $P_{O2} = 0.15$ Torr film. The spectra for the other films (grown under $P_{O2} = 0.1$, 0.05, and 0.03 Torr) are provided in the Supplemental Material (Fig. S3) [26]. The data were taken in the energy regions around the Co-K and Ni-K absorption edges (7.711 and 8.333 keV, respectively). Details of our model calculations are given in the Supplemental Material [26]. It is seen that our calculations reproduce well the experimentally observed profiles. We note that for the (022) reflection, a small dip at the Ni absorption edge, which would not be expected for the ideal inverse spinel structure, is obviously seen. This indicates that a small amount of Ni is included in the T_d site. Figures 3(a) and 3(b) show the cation compositions in the T_d and O_h sites determined by the model calculation. The composition of the $P_{O2} = 0.15$ Torr film was determined to be $(Co_{0.87}Ni_{0.13})(Co_{0.98}Ni_{1.02})O_4$. Figure 3(c) shows the P_{O2} dependence of the total amount of Ni ($x_{Td\text{-Ni}} + y_{Oh\text{-Ni}}$) in the films. We see that with increasing P_{O2}, the total amount of Ni in the films increases while the total amount of Co ($x_{Td\text{-Co}} + y_{Oh\text{-Co}}$) decreases. This implies that the ablated Co from the targets are preferentially scattered by the oxygen background gas [31]. In addition, the composition of the Ni occupying in the O_h site ($y_{Oh\text{-Ni}}$) becomes larger with increasing P_{O2} while the compositions of the Co and Ni in the T_d site ($x_{Td\text{-Co}}$ and $x_{Td\text{-Ni}}$) are less P_{O2} dependent and almost constant. Our observations indicate that depositing NCO

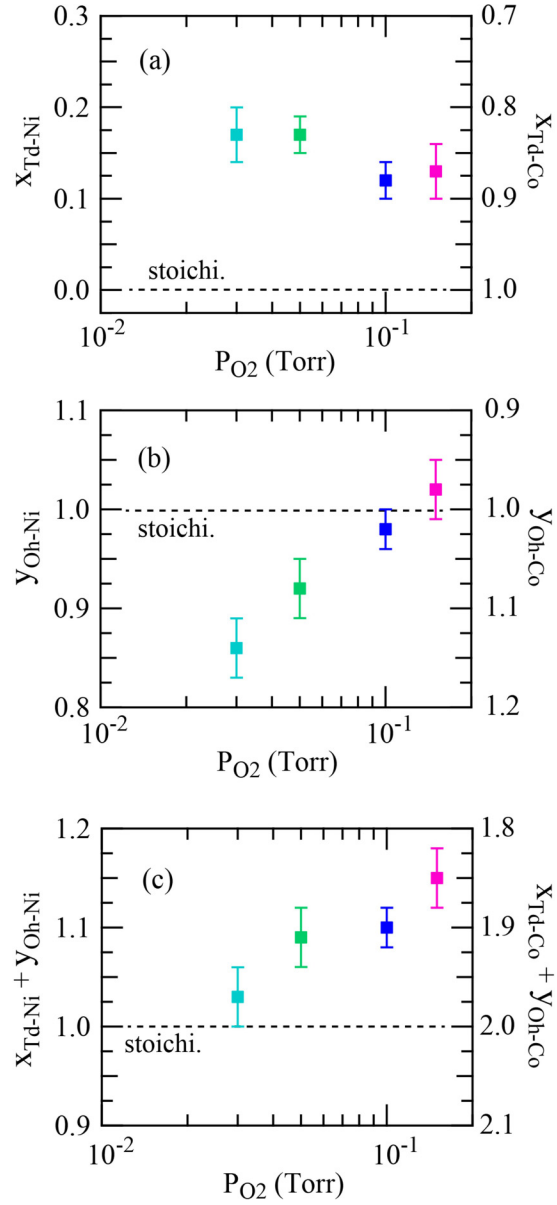

FIG. 3. (a), (b) P_{O2} dependence of the Ni composition in (a) T_d and (b) O_h sites of the NCO films. The composition of the NCO film is defined as $(Co_{x\text{-}Td\text{-Co}}Ni_{x\text{-}Td\text{-Ni}})\,(Co_{y\text{-}Oh\text{-Co}}Ni_{y\text{-}Oh\text{-Ni}})\,O_4$. The Co compositions in the T_d and O_h sites ($x_{Td\text{-Co}}$ and $y_{Oh\text{-Co}}$, respectively) are determined by assuming that $x_{Td\text{-Co}} + x_{Td\text{-Ni}} = 1$ and $y_{Oh\text{-Co}} + y_{Oh\text{-Ni}} = 2$. Details of the calculations are given in the Supplemental Material [26]. (c) P_{O2} dependence of the total Ni and Co composition in the films. The uncertainties (error bars) of the cation compositions were estimated with a threshold of 35% increase in the total squared error.

under higher P_{O2} stabilizes the octahedrally coordinated Ni and that P_{O2} is a key for controlling the cation distribution in the NCO films. It should be pointed out that the inverse spinel NCO has been shown theoretically to be half metallic and the density of states at the Fermi level consists of spin-down e_g electrons of the O_h site Ni [19,21,32]. This suggests that cation distribution, especially the O_h-site Ni concentration $y_{Oh\text{-Ni}}$ in the films, strongly influences magnetic and transport properties.

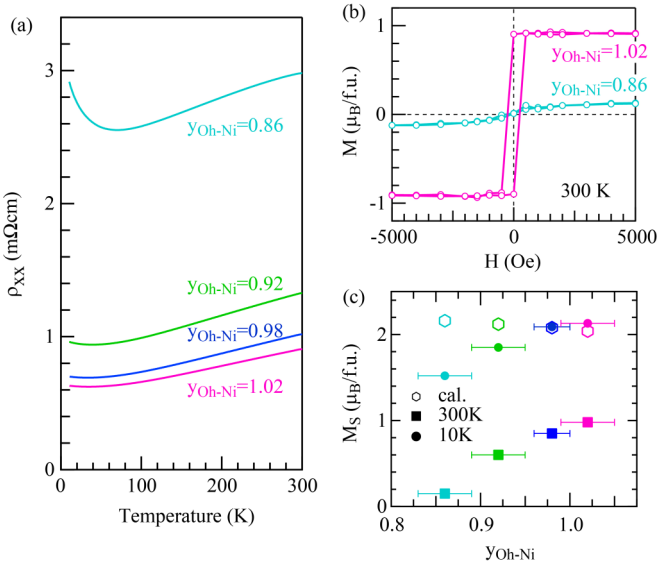

FIG. 4. (a) Temperature dependence of electrical resistivity for the NCO films with $y_{Oh\text{-}Ni} = 0.86$, 0.92, 0.98, and 1.02 (grown under $P_{O2} = 0.03$, 0.05, 0.1, and 0.15 Torr, respectively). (b) Room-temperature magnetic-field dependence of out-of-plane magnetization at 300 K for the $y_{Oh\text{-}Ni} = 0.86$ and 1.02 films. (c) Saturated out-of-plane magnetization at 10 and 300 K for the NCO films as a function of the Ni concentration in the O_h site $y_{Oh\text{-}Ni}$. The open circles correspond to the calculated magnetizations based on the experimentally determined cation distributions for each film. The uncertainties of the cation compositions lead to about 1% variations of the calculated magnetization.

We now look into how the cation distribution, especially $y_{Oh\text{-}Ni}$, in the films influences their transport and magnetic properties. Figure 4(a) shows the temperature dependence of the electrical resistivity ρ_{xx} of the films with $y_{Oh\text{-}Ni} = 0.86$, 0.92, 0.98, and 1.02 (grown under $P_{O2} = 0.03$, 0.05, 0.1, and 0.15 Torr, respectively). The ρ_{xx} is found to decrease with increasing $y_{Oh\text{-}Ni}$ (i.e., with increasing P_{O2}). While metallic electrical conduction is seen with decreasing temperature from 300 K, the upturn in the $\rho_{xx} - T$ curves is developed at low temperatures. The upturn behavior is obvious for the films grown under a lower P_{O2} and thus with a lower $y_{Oh\text{-}Ni}$, and the temperature at which the upturn behavior develops increases with decreasing $y_{Oh\text{-}Ni}$. This implies that the cation distribution significantly influences the electrical conductions in the films and that the upturn behavior probably is caused by disorders and defects related to the deviations of the O_h-cation distribution from the stoichiometric. Figure 4(b) displays the room-temperature field dependence of out-of-plane magnetization for the films with $y_{Oh\text{-}Ni} = 0.86$ and 1.02. Diamagnetic signals from the substrates were extracted by linearly fitting the data in larger field regions and subtracted from measured curves. The film with $y_{Oh\text{-}Ni} = 1.02$ is found to possess remnant magnetization as large as 1 μ_B/f.u., which is comparable to the saturated magnetization M_s. The field-induced magnetization reversal occurs sharply with the coercive field of 210 Oe. These behaviors are characteristics of perpendicularly magnetized films. In contrast, the remnant magnetization of the $y_{Oh\text{-}Ni} = 0.86$ film is almost zero, and the saturated magnetization is also largely reduced to 0.2 μ_B/f.u. The results indicate that the P_{O2}-induced variations in the $y_{Oh\text{-}Ni}$ impact the ferrimagnetic magnetizations and the perpendicular anisotropy in the films significantly. Figure 4(c) shows the saturated magnetization at 300 and 10 K as a function of $y_{Oh\text{-}Ni}$. The similar $y_{Oh\text{-}Ni}$ dependence was also confirmed for the magnetization extracted at the same relative temperature of $T = 0.5\,T_c$ (Supplemental Material, Figure S4a [26]). We also calculated the magnetization based on the experimentally determined cation distributions for each film. For the calculations, based on the ligand field stabilization energy, it is assumed that Co and Ni in the T_d sites have the +2 and +3 valence states, respectively, and both of them are in high-spin states ($S_{Co\text{-}Td} = 3/2$ and $S_{Ni\text{-}Td} = 3/2$) while both Co and Ni in the O_h sites have +3 valence states and are in low-spin states ($S_{Co\text{-}Oh} = 0$ and $S_{Ni\text{-}Oh} = 1/2$). This configuration corresponds to the one described in Fig. S1a in the Supplemental Material [26]. The spins between each T_d and O_h-site sublattices are coupled in the antiparallel configuration (corresponding to the ferrimagnetic interaction). As shown in the figure, the calculated magnetization is found to slightly increase when the $y_{Oh\text{-}Ni}$ decreases as a consequence of the fact that the compensation of the magnetization between the T_d and O_h sublattices diminishes. Despite the fact that magnetizations of the $y_{Oh\text{-}Ni} = 0.98$ and 1.02 films are comparable to the calculated ones, the expected trend is opposite to our observation under both 10 and 300 K that increasing $y_{Oh\text{-}Ni}$ leads to the enhancement in the films' magnetization, highlighting that cation distribution in the O_h site strongly influences magnetic interactions in NCO films. If we assume that the cation distribution does not affect the cations' valence states, the replacements of Ni ($S_{Ni\text{-}Oh} = 1/2$) with Co ($S_{Co\text{-}Oh} = 0$) in the O_h site probably break the ferrimagnetic interactions between the T_d-site Co and O_h-site Ni, and in turn result in antiparallel alignments of spins in the T_d sublattice, consequently reducing the total magnetization in the NCO film. Another possibility is that the valence states of the cations are changed depending on the cation distribution. To see these possibilities, x-ray absorption spectroscopy and x-ray magnetic circular dichroism spectroscopy will be necessary. These characterizations could provide insight on cation distribution and their influence on magnetic properties of spinel oxides [24]. In any case, our data show that the cation distributions in the films impact the stability of the ferrimagnetic ordering and the Co substitutions for Ni in the O_h sites make the ferrimagnetic ordering more unstable. In fact, the temperature dependence of the magnetization (Figure S4b in the Supplemental Material [26]) shows that the films with $y_{Oh\text{-}Ni} = 0.98$ and 1.02 have the ferrimagnetic transition temperature above 400 K and the transition temperature decreases with increasing the Co substitutions for Ni in the O_h sites. We also note that because the O_h-site Co provides no electron carriers, increasing the Co substitution in the films deteriorate their electrical conductions, which is in agreement with our observations [Fig. 4(a)]. It should be pointed out that oxygen vacancies might be a possible cause for the P_{O2} dependence of the films' properties. However, we found that postannealing the as-grown films under oxygen atmosphere is found to deteriorate their ferrimagnetic transition temperature and magnetization (Supplemental Material, Fig. S5 [26]).

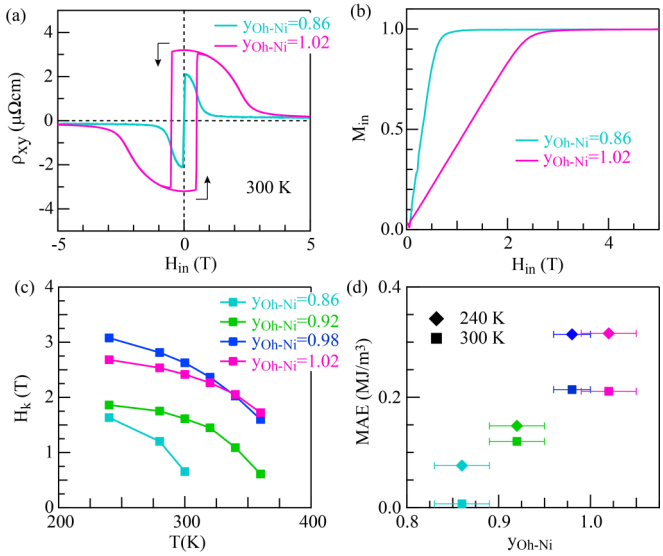

FIG. 5. (a) In-plane magnetic-field H_{in} dependence of the transverse resistivity ρ_{xy} for the $P_{O2} = 0.03$ Torr and 0.15 Torr films. (b) H_{in} dependence of the in-plane component of the normalized magnetization M_{in}, extracted from the H_{in}-ρ_{xy} curves in (a). (c) Temperature dependence of the anisotropy field H_k for the NCO films. (d) $y_{Oh\text{-}Ni}$ dependence of the perpendicular anisotropy energy (MAE) of the NCO films at 300 and 240 K.

If oxygen vacancies would play key roles in the magnetic properties in the NCO films, the magnetic properties of the annealed films should be similar to those for the films grown under larger P_{O2}. This expectation is contrary to our experimental observations (Fig. S5), indicating that the influence of oxygen vacancies on the properties are less dominant and the oxygen pressure during the film growth determines the cation distribution, not the oxygen vacancy concentration in the films.

We also characterize the influence of the cation distribution on the perpendicular anisotropy in the films. To quantitatively evaluate the anisotropy, we applied the in-plane magnetic field H_{in} (parallel to the excitation current along the longitudinal direction of the Hall bar) and measured the transverse (Hall) resistivity ρ_{xy}. In this measurement configuration, the field-induced ordinary Hall effect is negligibly small and thus the measured ρ_{xy} is considered to originate only from the anomalous Hall effect, which gives rise to the transverse resistivity proportional to the perpendicular component of the magnetization. Figure 5(a) shows the room-temperature H_{in} dependence of ρ_{xy} for the $y_{Oh\text{-}Ni} = 1.02$ and 0.86 films. For both films, ρ_{xy} is almost zero in large positive-H_{in} ($\sim$5 T) region and as the H_{in} is swept downward, the ρ_{xy} gradually increases and is maximized at 0 T. This behavior can be understood by considering that the films have a perpendicular magnetization and the magnetization gradually tilts toward the in-plane direction with increasing H_{in}. Because a small perpendicular component of the external field exists due to misalignments of the in-plane field (the uncertainty of the field angle was $\pm 1^\circ$), the films have the single ferrimagnetic domain state and have the maximized ρ_{xy} at 0 T. This also explains the occurrence of the switching of the ρ_{xy}'s sign in the negative-H_{in} region. In the return sweep from the negative field to the positive field, essentially the same magnetization processes are seen. We note that while the overall behaviors of ρ_{xy} in one film is similar to those in any others, the in-plane magnetic fields at which the ρ_{xy} becomes zero and the switching between the positive and negative ρ_{xy} occurs strongly depend on $y_{Oh\text{-}Ni}$, revealing the strong impact of the cation distribution on the perpendicular magnetic anisotropy.

To determine the saturation field and the perpendicular anisotropy energy, we converted the ρ_{xy}-H_{in} curves into the H_{in} dependence of the in-plane component of the normalized magnetization M_{in} by taking $M_{in} = \sin[\cos^{-1}(\rho^n{}_{xy})]$, where $\rho^n{}_{xy}$ is the transverse resistivity normalized by the value at 0 T. The extracted M_{in}-H_{in} curves for the $y_{Oh\text{-}Ni} = 0.86$ and 1.02 films are shown in Fig. 5(b). The anisotropy field H_k, which is defined as the magnetic field necessary to align the magnetization along the in-plane direction and is calculated as $H_k = 2\int H_{in} dM_{in}$, is 0.65 T for the $y_{Oh\text{-}Ni} = 0.86$ film and 2.42 T for $y_{Oh\text{-}Ni} = 1.02$ at room temperature, indicating that the O_h-site Ni plays an important role in stabilizing the perpendicular anisotropy in the films. This is further confirmed from the temperature dependence of the H_k for the films in Fig. 4(c). Although the H_k of each of the films ($y_{Oh\text{-}Ni} = 0.86$, 0.92, 0.98, 1.02) decreases as the temperature approaches the ferrimagnetic transition temperature, the magnitude of H_k increases with increasing $y_{Oh\text{-}Ni}$ in the films. For the films with the larger $y_{Oh\text{-}Ni}$, whose cation compositions are close to the stoichiometric, the relatively large H_k are maintained even in the high-temperature region (H_k at 360 K $\sim$ 2 T). We also evaluate the perpendicular magnetic anisotropy energy (MAE) by taking MAE $= M_s H_k/2$. Figure 5(d) shows the $y_{Oh\text{-}Ni}$ dependence of the room-temperature MAE. As expected, the MAE follows the trend similar to the $y_{Oh\text{-}Ni}$ dependence of the H_k. The MAE increases with increasing $y_{Oh\text{-}Ni}$ and is almost saturated when the cation distribution is close to the stoichiometric. The films with the cation distribution close to the stoichiometric have MAE as large as 0.2 MJ/m^3 at room temperature. Given that orbital magnetic moment ties closely to magnetic anisotropy through spin-orbit interactions [33–35], the observed $y_{Oh\text{-}Ni}$ dependence of the H_k and MAE implies that the O_h-site Ni composition is a key for introducing and increasing the perpendicular component of the orbital magnetic moment, stabilizing the perpendicular anisotropy.

IV. SUMMARY

We quantitatively evaluated the cation distribution in $NiCo_2O_4$ thin films epitaxially grown by pulsed laser deposition and comprehensively delineated how the distribution impacts their ferrimagnetism and perpendicular magnetic anisotropy. We found that the Ni concentration in the O_h-site $y_{Oh\text{-}Ni}$ can be tuned by simply adjusting the oxygen partial pressure P_{O2} during the film growth and such P_{O2}-induced changes in $y_{Oh\text{-}Ni}$ impact the ferrimagnetism and the magnetic anisotropy. The films whose cation distributions are close to the stoichiometric exhibit ferrimagnetism with a transition temperature higher than 400 K and enhanced perpendicular magnetic anisotropy. On the other hand, these ferrimagnetic properties are found to deteriorate with reduced $y_{Oh\text{-}Ni}$. Our

results demonstrate that tuning the cation distribution is a way to control the ferrimagnetism and the anisotropy of $NiCo_2O_4$, providing a degree of freedom in designing spintronic devices based on spinel oxides.

ACKNOWLEDGMENTS

This work was partially supported by a grant for the Integrated Research Consortium on Chemical Sciences, by Grants-in-Aid for Scientific Research (Grants No. JP16H02266, No. JP17H05217, No. JP17H04813, and No. JP19H05816), by a JSPS Core-to-Core program (A), and by a grant for the Joint Project of Chemical Synthesis Core Research Institutions from the Ministry of Education, Culture, Sports, Science and Technology (MEXT) of Japan. The synchrotron radiation experiments at the Photon Factory were performed with the approval of the Photon Factory Program Advisory Committee (Proposal No. 2018G533).

[1] J. D. Dunitz and L. E. Orgel, J. Phys. Chem Solids **3**, 318 (1957).
[2] X. Batlle, X. Obradors, J. Rodríguez-Carvajal, M. Pernet, M. V. Cabañas, and M. Vallet, J. Appl. Phys. **70**, 1614 (1991).
[3] E. J. W. Verwey, F. D. Boer, and J. H. V. Santen, J. Chem. Phys. **16**, 1091 (1948).
[4] A. Zakutayev, T. R. Paudel, P. F. Ndione, J. D. Perkins, S. Lany, A. Zunger, and D. S. Ginley, Phys. Rev. B **85**, 085204 (2012).
[5] T. R. Paudel, A. Zakutayev, S. Lany, M. d'Avezac, and A. Zunger, Adv. Funct. Mater. **21**, 4493 (2011).
[6] S. Tripathy, D. S. Saini, and D. Bhattacharya, J. Asian Ceram. Soc. **4**, 149 (2016).
[7] R. Zhang, Q. Yuan, R. Ma, X. Liu, C. Gao, M. Liu, C.-L. Jia, and H. Wang, RSC Adv. **7**, 21926 (2017).
[8] P. F. Ndione, Y. Shi, V. Stevanovic, S. Lany, A. Zakutayev, P. A. Parilla, J. D. Perkins, J. J. Berry, D. S. Ginley, and M. F. Toney, Adv. Funct. Mater. **24**, 610 (2014).
[9] D. Das and S. Ghosh, J. Phys.: Condens. Matter **29**, 055805 (2016).
[10] J. F. Marco, J. R. Gancedo, M. Gracia, J. L. Gautier, E. Ríos, and F. J. Berry, J. Solid State Chem. **153**, 74 (2000).
[11] D. Pyke, K. K. Mallick, R. Reynolds, and A. K. Bhattacharya, J. Mater. Chem. **8**, 1095 (1998).
[12] O. Knop, K. I. G. Reid, Sutarno, and Y. Nakagawa, Can. J. Chem. **46**, 3463 (1968).
[13] P. D. Battle, A. K. Cheetham, and J. B. Goodenough, Mater. Res. Bull. **14**, 1013 (1979).
[14] J. F. Marco, J. R. Gancedo, M. Gracia, J. L. Gautier, E. I. Ríos, H. M. Palmer, C. Greaves, and F. J. Berry, J. Mater. Chem. **11**, 3087 (2001).
[15] J. Zhu and Q. Gao, Microporous Mesoporous Mater. **124**, 144 (2009).
[16] D. P. Dubal, P. Gomez-Romero, B. R. Sankapal, and R. Holze, Nano Energy **11**, 377 (2015).
[17] R. Ding, L. Qi, M. Jia, and H. Wang, Nanoscale **6**, 1369 (2014).
[18] M. U. Anu Prathap and R. Srivastava, Nano Energy **2**, 1046 (2013).
[19] K. Zhang, C. Zhen, W. Wei, W. Guo, G. Tang, L. Ma, D. Hou, and X. Wu, RSC Adv. **7**, 36026 (2017).
[20] C. Zhen, X. Zhang, W. Wei, W. Guo, A. Pant, X. Xu, J. Shen, L. Ma, and D. Hou, J. Phys. D: Appl. Phys. **51**, 145308 (2018).
[21] M. Wang, X. Sui, Y. Wang, Y.-H. Juan, Y. Lyu, H. Peng, T. Huang, S. Shen, C. Guo, J. Zhang, Z. Li, H.-B. Li, N. Lu, A. T. N'Diaye, E. Arenholz, S. Zhou, Q. He, Y.-H. Chu, W. Duan, and P. Yu, Adv. Mater. **31**, 1900458 (2019).
[22] X. Chen, X. Zhang, M.-G. Han, L. Zhang, Y. Zhu, X. Xu, and X. Hong, Adv. Mater. **31**, 1805260 (2019).
[23] P. Silwal, C. La-o-vorakiat, E. E. M. Chia, D. H. Kim, and D. Talbayev, AIP Adv. **3**, 092116 (2013).
[24] Y. Bitla, Y.-Y. Chin, J.-C. Lin, C. N. Van, R. Liu, Y. Zhu, H.-J. Liu, Q. Zhan, H.-J. Lin, C.-T. Chen, Y.-H. Chu, and Q. He, Sci. Rep. **5**, 15201 (2015).
[25] P. Silwal, L. Miao, I. Stern, X. Zhou, J. Hu, and D. H. Kim, Appl. Phys. Lett. **100**, 032102 (2012).
[26] See Supplemental Material at http://link.aps.org/supplemental/10.1103/PhysRevB.101.094412 for possible variations in cation valence state in $NiCo_2O_4$, details of x-ray structural characterizations, structural model calculations, and magnetic property characterizations.
[27] M. De Santis, A. Bailly, I. Coates, S. Grenier, O. Heckmann, K. Hricovini, Y. Joly, V. Langlais, A. Y. Ramos, C. Richter, X. Torrelles, S. Garaudee, O. Geaymond, and O. Ulrich, Acta Crystallogr. Sect. B **75**, 8 (2019).
[28] T.-Y. Koo, D.-S. Lee, and J. Song, J. Korean Phys. Soc. **65**, 1547 (2014).
[29] C. Lefevre, A. Thomasson, F. Roulland, V. Favre-Nicolin, Y. Joly, Y. Wakabayashi, G. Versini, S. Barre, C. Leuvrey, A. Demchenko, N. Boudet, and N. Viart, J. Appl. Crystallogr. **49**, 1308 (2016).
[30] C. Lefevre, A. Demchenko, C. Bouillet, M. Luysberg, X. Devaux, F. Roulland, G. Versini, S. Barre, Y. Wakabayashi, N. Boudet, C. Leuvrey, M. Acosta, C. Meny, E. Martin, S. Grenier, V. Favre-Nicolin, and N. Viart, Small Methods **1**, 1700234 (2017).
[31] S. Wicklein, A. Sambri, S. Amoruso, X. Wang, R. Bruzzese, A. Koehl, and R. Dittmann, Appl. Phys. Lett. **101**, 131601 (2012).
[32] P. Li, C. Xia, D. Zheng, P. Wang, C. Jin, and H. Bai, Phys. Status solidi (RRL) **10**, 190 (2016).
[33] D. Weller, J. Stöhr, R. Nakajima, A. Carl, M. G. Samant, C. Chappert, R. Mégy, P. Beauvillain, P. Veillet, and G. A. Held, Phys. Rev. Lett. **75**, 3752 (1995).
[34] N. Nakajima, T. Koide, T. Shidara, H. Miyauchi, H. Fukutani, A. Fujimori, K. Iio, T. Katayama, M. Nývlt, and Y. Suzuki, Phys. Rev. Lett. **81**, 5229 (1998).
[35] P. Bruno, Phys. Rev. B **39**, 865 (1989).